Journal of Anatomy

J. Anat. (2009) **214**, pp817–829 doi: 10.1111/j.1469-7580.2009.01073.x

Anticipating bipedalism: trabecular organization in the newborn ilium

Craig A. Cunningham and Sue M. Black

Centre for Anatomy and Human Identification, College of Life Sciences, University of Dundee, Scotland, UK

Abstract

Trabecular bone structural organization is considered to be predominantly influenced by localized temporal forces which act to maintain and remodel the trabecular architecture into a biomechanically optimal configuration. In the adult pelvis, the most significant remodelling forces are believed to be those generated during bipedal locomotion. However, during the fetal and neonatal period the pelvic complex is non-weight bearing and, as such, structural organization of iliac trabecular bone cannot reflect direct stance-related forces. In this study, micro-computed tomography scans from 28 neonatal ilia were analysed, using a whole bone approach, to investigate the trabecular characteristics present within specific volumes of interest relevant to density gradients highlighted in a previous radiographic study. Analysis of the structural indices bone volume fraction, trabecular thickness, trabecular spacing and trabecular number was carried out to quantitatively investigate structural composition. Quantification of the neonatal trabecular structure reinforced radiographic observations by highlighting regions of significant architectural form which grossly parallel architectural differences in the adult pattern but which have previously been attributed to stance-related forces. It is suggested that the seemingly organized rudimentary scaffold observed in the neonatal ilium may be attributable to other non-weight bearing anatomical interactions or even to a predetermined genetic blueprint. It must also be postulated that whilst the observed patterning may be indicative of a predetermined inherent template, early non-weight bearing and late stance-related locomotive influences may subsequently be superimposed upon this scaffolding and perhaps reinforced and likely remodelled at a later age. Ultimately, the analysis of this fundamental primary pattern has core implications for understanding the earliest changes in pelvic trabecular architecture and provides a baseline insight into future ontogenetic development and bipedal capabilities.

Key words trabecular architecture; quantitative analysis; ilium; juvenile; micro-computed tomography.

Introduction

The relationship between bone form and function is well understood and has been investigated extensively in early studies from the 19th century (Ward, 1838; Von Mayer, 1867; Wolff, 1892, 1986; Evans, 1957), through seminal work in the past decades (Evans, 1973; Lanyon, 1974; Carter & Hayes, 1977; Gibson, 1985; Goldstein, 1987; Frost, 1990; Ciarelli et al. 1991; Biewener et al. 1996), to current research (Keaveny et al. 2001; Jee, 2005; Liu et al. 2006; Gosman & Ketcham, 2008). However, the knowledge of bone biomechanics and the specialized micro anatomy of trabecular characteristics has expanded exponentially over the past two decades with complex studies addressing the continuous modification and alteration of internal bone structure (Compston, 2006; Müller & Van Lenthe, 2006). With this expansion in knowledge there has been a greater understanding of the trabecular changes which occur in response to development (Nuzzo et al. 2003; Ryan & Krovitz, 2006; Gosman & Ketcham, 2008), ageing (Macho et al. 2005; Muller, 2005; Stauber & Muller, 2006, Nagaraja et al. 2007), bone biochemistry (Ripamonti, 2006) and therapeutic intervention (Ding et al. 2003; Pierroz et al. 2006). Traditionally, histomorphometric techniques performed on two-dimensional sections were recognized as the gold standard for the assessment and calculation of trabecular characteristics (Saparin et al. 2006) with occasional extrapolation to the third spatial dimension using various model assumptions of trabecular bone (Parfitt et al. 1987). These histomorphometric techniques were based on the use of optical microscopy

Correspondence
Craig Cunningham, University of Dundee, Centre for Anatomy and Human Identification, College of Life Sciences, Dow Street, Dundee, Scotland, UK DD1 5EH. T: + 44 (01382 388830;
E: c.a.cunningham@dundee.ac.uk

Accepted for publication *16 February 2009*

and the principles of quantitative histology and stereology (Dalle Carbonare et al. 2005). However, there has been a noticeable and steady shift from these time-consuming techniques to the more widely used and accepted imaging modalities, which are specifically designed to assess three-dimensional microstructures at high resolution and have the benefit of being non-destructive (Genant et al. 2000; Jones et al. 2007). This high degree of spatial resolution coupled with the possibility to observe the internal structure via non-destructive techniques has made it possible to investigate previously inaccessible rare skeletal material (Cunningham & Black, 2009) where destructive analysis was forbidden due to the uniqueness and value of the material involved. The introduction of three-dimensional imaging techniques and associated software, which have the capabilities of handling large datasets and calculating complex trabecular characteristics, have been instrumental in the development of knowledge into the microenvironment of trabecular architecture. The imaging technique of choice for trabecular bone analysis is micro-computed tomography (Qin et al. 2007), an imaging modality which can visualize the internal structure of intact bones with a high degree of spatial resolution and provide an efficient and reliable means by which 3D architecture can be quantified (Cooper et al. 2003). However, although the knowledge of trabecular architecture has increased as a direct result of these imaging techniques, studies have generally been confined to animal models due to the size restrictions imposed by the capability of the imaging systems. This has prompted many studies to investigate trabecular architecture using rodent models and in particular the detailed knowledge of bone disease, such as osteoporosis, has increased considerably as investigators can manually control variables such as endocrine influences (Laib et al. 2001; Boyd et al. 2006) or induced stresses (Nakano et al. 2003), thereby assessing changing structural parameters in a longitudinal study. Studies of this kind in the human have been restricted to clinical and post-mortem trephined bone samples taken from various anatomical sites including the vertebrae, iliac crest, and calcaneus (Moore et al. 1989; Chappard et al. 1999; Hildebrand et al. 1999; Glorieux et al. 2000; Thomsen et al. 2002). This is restrictive as only limited anatomical regions can be accessed and an assessment of overall trabecular bone structure cannot be gained. Studies involving whole bone analysis have been curtailed due to micro CT apparatus size restrictions and the fact that with an increased field of view, which is inherent to whole bone analysis, there is a resultant and directly related decrease in image resolution (Kim et al. 2004). This is also the case for clinical CT, as although whole bones can be scanned, even the highest resolution multislice clinical CT scanner cannot produce scan resolutions which are capable of resolving the smallest trabeculae (Patel et al. 2005; Petersson et al. 2006). Only recently have technological advances in micro-computed tomography apparatus allowed for scanners to be produced with gantry sizes capable of accommodating much larger sample sizes coupled with a maintained high spatial resolution (Müller et al. 1998; Ritman, 2004; Stauber & Müller, 2008) in the range required for trabecular visualization (Whitehouse, 1974; Chappard et al. 1999; Byers et al. 2000). With this advance, studies have been able to investigate the ontogenetic development of the complete trabecular architecture within various human bones (Ryan & Krovitz, 2006; Gosman & Ketcham, 2008). However, although the potential is now available for such studies, the paucity of provenanced juvenile material remains restrictive to the advancement of this fundamental area of skeletal biology. As a result, a significant portion of research remains directed to phylogenetic variation in primates (Fajardo & Muller, 2001; Fajardo et al. 2002; Ryan & Ketcham, 2002; Ryan & van Rietbergen, 2005).

Ontogenetic studies of trabecular architecture are important for furthering our understanding of the mechanical properties of bone as during life, bone develops into a load-bearing structure (Mulder et al. 2007) requiring the trabecular architecture to be arranged structurally to accommodate and remodel in response to a life-time of changing stresses (Martinon-Torres, 2003). This structural arrangement is fundamentally important as trabecular architecture has been shown to have a significant role in bone strength and in determining its fundamental biomechanical properties (Majumdar et al. 1998; Ulrich et al. 1999; Muller, 2005; Bevill et al. 2006).

The pelvis is an area within the skeleton which undergoes continually changing stresses throughout development, therefore making it a functionally significant region for investigating ontogenetic trabecular structure. As few studies have considered the pelvic complex as a discrete entity due to its shape and complex structural architecture (Majumder et al. 2004), little is known about the changes to the internal developing structure (Dalstra et al. 1993). As such, this study will investigate the following trabecular parameters: bone volume fraction (BV/TV), trabecular thickness (Tb.Th), trabecular number (Tb.N) and trabecular separation (Tb.S) in the neonatal human ilium as a baseline template prior to considering change in relation to the growing child.

In a previous communication (Cunningham & Black, 2009), the gross structural parameters within the neonatal ilium demonstrated an unexpected early trabecular organization which was considered in terms of associated anatomy and functional forces acting during the fetal and neonatal periods of development. This seemingly precocious structural patterning also prompted a reconsideration of the contribution biomechanical influences, in response to bipedalism, makes in securing the pelvic complex as a structurally optimized junctional complex for weight transfer in later years.

Materials and methods

Specimens

Twenty-eight neonatal ilia (15 right and 13 left from 16 individuals) were selected and analysed from the Scheuer Collection of juvenile skeletal remains, housed within the Centre for Anatomy and Human Identification, University of Dundee. Specimens were confirmed as occupying the neonatal developmental period via metric evaluations of the ilium (Fazakas & Kosa, 1978). All specimens were free from any visible external damage which might have affected the underlying trabecular architecture. Information pertaining to the provenance and demography of this collection has been documented previously (Scheuer & Black, 2000; Cunningham & Black, 2009).

MicroCT imaging

Each specimen was scanned at the University of Hull, Centre for Medical and Engineering Technology (CMET) using an X-Tek HMX 160 micro-computed tomography scanner (X-Tek Systems Ltd, Tring, UK) at voltage (84 kV), current (17 μA) with an aperture setting of 50%. In preparation for scanning, each specimen was attached in an upright position to a carbon fibre plate, which was then positioned vertically in the μCT system. During the scanning process the sample was rotated through 360° in typically 1300 steps, with a 2D image collected at each step. Extraneous noise in the images was minimized by taking 16 images at each scanning step and averaging the results. Image reconstruction, whereby the digitized 2D X-ray images were converted into a 3D volumetric structure, was performed using NGI CT Control software (X-Tek, Tring, UK). From this volume an image stack was created for which the resultant slice pixel size ranged between 34.5 and 44 μm dependent on sample size. After completion of the scanning process and image reconstruction, 2D μCT slice images were exported as a stack of 16-bit tiff (Tagged Image File Format) images.

Analysis software

Analysis of μCT data was performed using CTAnalyser (*CTAn*), a 2D visualization and 2D/3D analysis software provided by SkyScan. CTAn is a visualization and quantification application for two-dimensional and three-dimensional data which compliments micro-computed tomography systems by offering a number of visualization and analysis tools applying model-independent stereological principles to microCT data. In this study, all parameters are measured in three dimensions. The following histomorphometric parameters of trabecular bone were calculated using CTAn.

Bone volume fraction (BV/TV)

BV/TV is a measure of the trabecular bone volume in relation to the total reference volume represented as a percentage. Trabecular bone volume fraction is one of the most important and fundamental architectural properties of cancellous bone (Ding et al. 1999). This parameter is only relevant if studied within a biphasic region of solid and space, such as a trabecular bone region, and must not include any region of cortical bone.

Trabecular thickness (Tb.Th)

Trabecular thickness was determined as an average of the local thickness at each voxel representing binarized bone (Ulrich et al. 1999). Hildebrand & Ruegsegger (1997) defined the local thickness for a point in solid as the diameter of a sphere, where the sphere encloses the point and is entirely bounded within the solid surface. A single mean value for trabecular thickness from a volume of interest is commonly reported and is how Tb.Th was measured in this study. The values for trabecular thickness are represented in mm.

Trabecular separation (Tb.Sp)

Trabecular separation is a measure of the average thickness of space between trabecular struts as defined by binarization within the volume of interest. Trabecular separation is calculated independently in three dimensions using the same method outlined for measurement of trabecular thickness. The values for trabecular separation are expressed in mm.

Trabecular number (Tb.N)

Trabecular number is a measure of the number of traversals across a trabecular or solid structure made per unit length on a linear path through a trabecular bone region. The complexities of model dependence are eliminated by the true three-dimensional calculation of Tb.N from μCT images. Trabecular number is measured by the application of the eq. 1 for a parallel plate model of trabecular structure.

$$\mathrm{Tb.N} = (\mathrm{BV/TV})/\mathrm{Tb.Th} \quad (1)$$

The values for trabecular number are expressed in mm^{-1}.

Selection of volumes of interest (VOIs)

Within the ilium, 23 volumes of interest (VOI 1–23) were selected based on a uniform grid which was superimposed onto the iliac surface using specific anatomical points of reference (Fig. 1). Best efforts were made to position the grid so that comparable volumes of interest could be analysed between specimens. It is acknowledged that there may be some degree of variation between individuals; however, it is suggested that this variation is minimal due to all ilia occupying the same developmental group and as such having very similar size and shape. To identify and select the analysis field within a particular VOI, an elliptic volume was selected and placed in the appropriate grid position within a biphasic region and interpolated throughout the 3D dataset for each grid square. Once the VOI was in an appropriate position, bone parameters were calculated. The VOIs analysed are defined in Fig. 1 and their regional descriptions shown in Fig. 2.

Statistics

Descriptive statistics were obtained for all variables within each VOI (Table 1). SigmaStat was used to perform an analysis of variance (anova) test between all VOIs for each structural parameter. For non-parametric data, a Kruskal–Wallis one way analysis of variance on ranks test was used. This test was used to determine overall significance between VOIs. Once overall significance was established, pairwise multiple comparison procedures were performed to determine significance between individual VOIs for each structural parameter. For non-parametric data, Dunn's method was used. This test lists the difference of rank means, computes the Q test statistic, and displays whether $P < 0.05$ for each parameter pair. Due to the volume of data produced and to permit an ease of

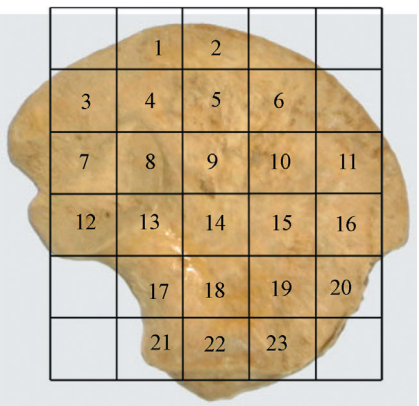

Fig. 1 Image of human neonatal ilium illustrating positioning of volumes of interest (VOI).

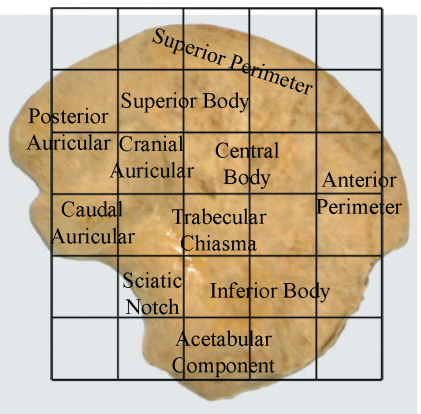

Fig. 2 Image of neonatal ilium documenting descriptive terminology in relation to volumes of interest.

interpretation, summarized statistical significance between VOIs from these procedures is displayed in Table 2A–D.

Results

Trabecular structural parameters were obtained from computed analysis of three-dimensional slice data produced from micro-computed tomography. Table 1 documents the descriptive statistics of the neonatal iliac trabecular parameters. Analysis of variance highlighted an overall significant difference between VOIs for each structural parameter. As such, pairwise multiple comparisons further investigated relationships between individual regions. For statistical significance between each VOI see Table 2A–D. Descriptions of trabecular morphology will be based upon the regional terminology shown in Fig. 2. Descriptions of regional trabecular morphology have been divided into groups with statistically similar values to aid understanding.

Bone volume fraction (BV/TV)

Bone volume fraction for the neonatal ilium has been divided into three distinct regional groupings based on

Table 1 Descriptive statistics (mean ± SD) of trabecular architectural parameters at each volume of interest (VOI)

VOI	BV/TV (%)	Tb.Th (mm)	Tb.Sp (mm)	Tb.N (mm^{-1})
1	36.891 ± 3.639	0.146 ± 0.014	0.226 ± 0.026	2.533 ± 0.197
2	40.377 ± 3.865	0.148 ± 0.012	0.210 ± 0.018	2.723 ± 0.201
3	37.820 ± 4.776	0.162 ± 0.009	0.244 ± 0.025	2.335 ± 0.283
4	33.460 ± 5.105	0.169 ± 0.012	0.304 ± 0.053	1.995 ± 0.374
5	34.415 ± 4.179	0.148 ± 0.010	0.252 ± 0.035	2.338 ± 0.302
6	35.655 ± 4.245	0.145 ± 0.013	0.230 ± 0.018	2.460 ± 0.242
7	34.866 ± 3.897	0.174 ± 0.012	0.291 ± 0.032	2.011 ± 0.221
8	26.734 ± 3.034	0.175 ± 0.009	0.380 ± 0.058	1.538 ± 0.208
9	21.710 ± 3.898	0.156 ± 0.016	0.359 ± 0.067	1.405 ± 0.292
10	30.857 ± 5.224	0.148 ± 0.012	0.270 ± 0.036	2.087 ± 0.325
11	37.655 ± 4.950	0.150 ± 0.009	0.225 ± 0.024	2.514 ± 0.300
12	33.022 ± 3.031	0.223 ± 0.021	0.414 ± 0.063	1.492 ± 0.188
13	31.953 ± 4.206	0.220 ± 0.016	0.433 ± 0.072	1.457 ± 0.205
14	18.909 ± 2.927	0.209 ± 0.021	0.548 ± 0.112	0.907 ± 0.138
15	19.013 ± 3.600	0.186 ± 0.024	0.509 ± 0.097	1.046 ± 0.283
16	41.044 ± 3.813	0.157 ± 0.011	0.225 ± 0.031	2.630 ± 0.269
17	25.998 ± 3.660	0.204 ± 0.019	0.455 ± 0.070	1.277 ± 0.169
18	29.126 ± 4.695	0.166 ± 0.012	0.328 ± 0.051	1.763 ± 0.285
19	30.021 ± 5.536	0.165 ± 0.011	0.317 ± 0.048	1.816 ± 0.327
20	25.659 ± 4.440	0.168 ± 0.021	0.341 ± 0.057	1.546 ± 0.321
21	42.751 ± 6.326	0.151 ± 0.013	0.218 ± 0.025	2.818 ± 0.392
22	39.374 ± 5.208	0.153 ± 0.012	0.239 ± 0.025	2.583 ± 0.302
23	43.475 ± 4.268	0.157 ± 0.011	0.220 ± 0.026	2.770 ± 0.273

Table 2 Pairwise multiple comparison of parameters between individual volumes. Non-parametric data were produced using Dunn's test. Statistical output has been summarized to illustrate which volumes are statistically similar, as such, Y, significant difference; N, no significant difference. Regional groupings have been coloured to aid interpretation. (A) High (yellow), medium (green), low (blue) bone volume fraction (BV/TV). (B) High (yellow), medium (green), low (blue) trabecular thickness (Tb.Th). (C) High (yellow), medium (green), low (blue) trabecular separation (Tb.Sp). (D) High (yellow), medium (green), low (blue) trabecular number (Tb.N)

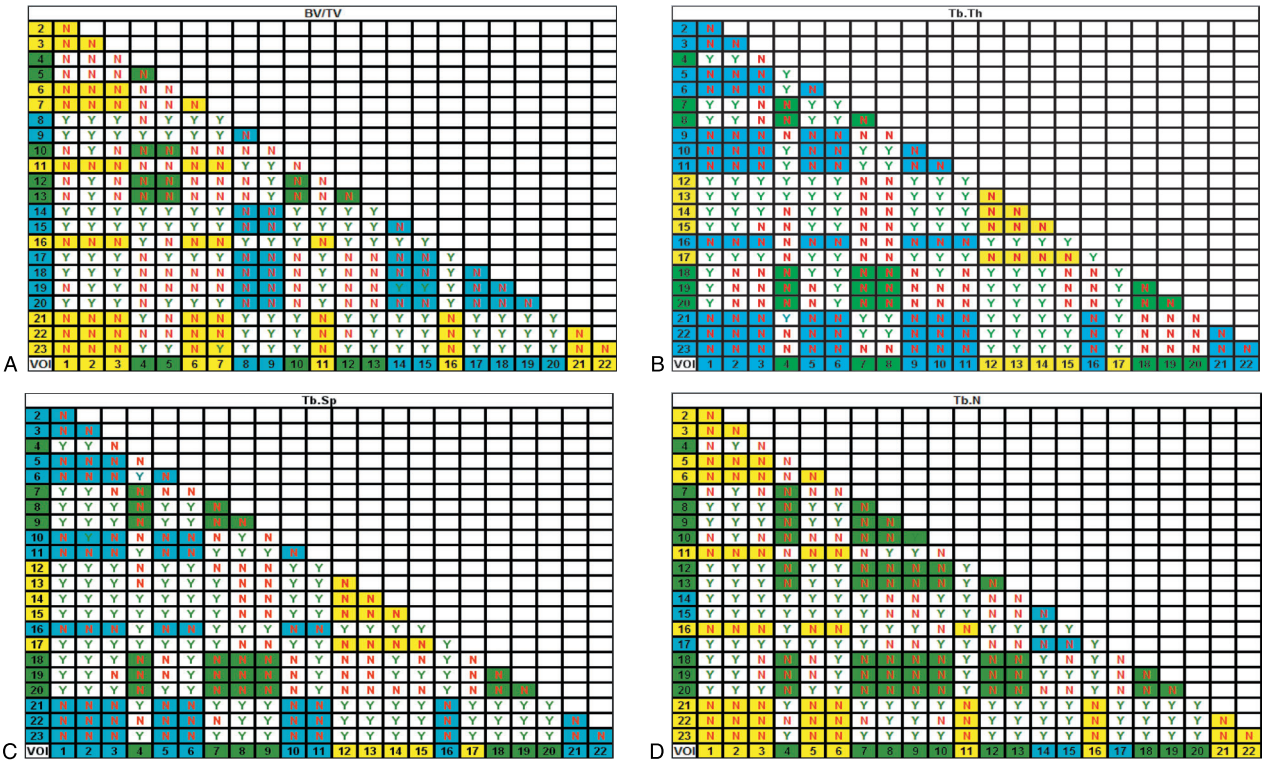

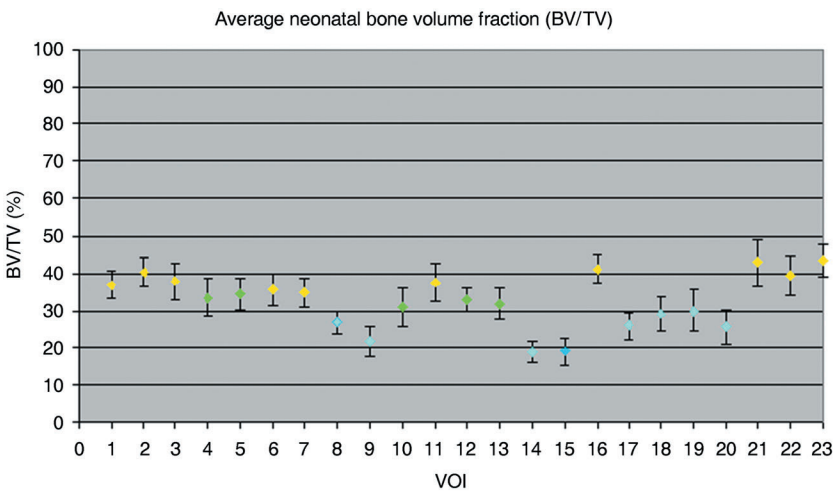

Fig. 3 Graphic representation of mean (± SD) bone volume fraction at each volume of interest.

the percentage bone volume observed within volumes of interest (Figs 3 and 7A). Volumes of interest contributing to a single group display no statistical difference between each other, with minor negligible exceptions (Table 2A). The regional grouping which displayed highest bone volume fraction comprised volumes corresponding to the superior perimeter (VOI 1, 2 and 6), posterior auricular (VOI 3 and 7), anterior perimeter (VOI 11 and 16) and acetabular regions (VOI 21–23). A decrease in BV/TV was observed in the superior body of the ilium (VOI 4 and 5), anterior central body (VOI 10) and at the caudal limb of the auricular surface (VOI 12 and 13). A further decrease in

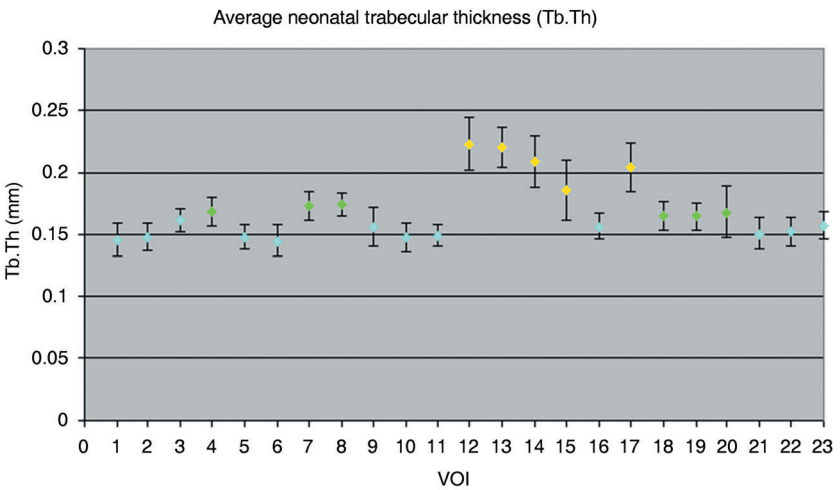

Fig. 4 Graphic representation of mean (± SD) trabecular thickness at each volume of interest.

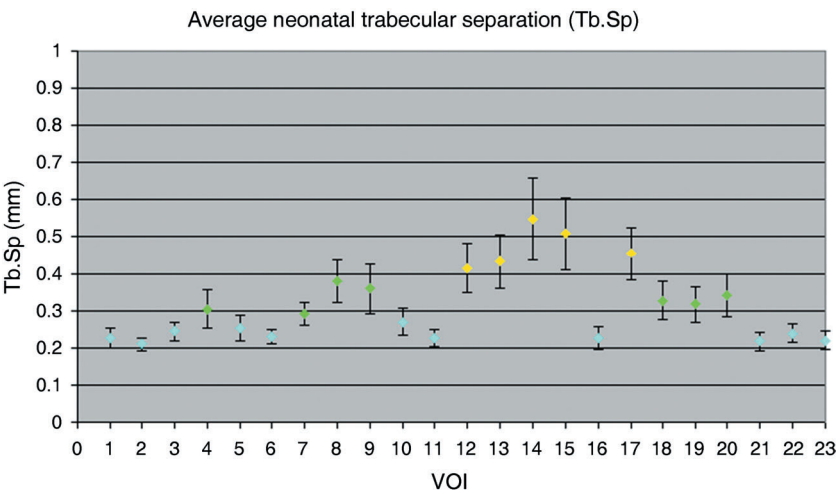

Fig. 5 Graphic representation of mean (± SD) trabecular separation at each volume of interest.

BV/TV was observed in the cranial auricular surface (VOI 8), central body of the ilium (VOI 9), the trabecular chiasma region (VOI 14 and 15), greater sciatic notch region (VOI 17), and inferior body (VOI 18–20).

Trabecular thickness (Tb.Th)

Trabecular thickness within the neonatal ilium can be defined by three different groupings (Figs 4 and 7B). There is no statistical difference between volumes of interest contributing to a single group (Table 2B). The first of these regional groupings is observed in the superior perimeter (VOI 1, 2 and 6), posterior auricular region (VOI 3), superior and central body (VOI 5, 9 and 10), anterior perimeter (VOI 11 and 16), and the acetabular component (VOI 21–23). Increased trabecular thickness volumes are located in the cranial limb of the auricular surface (VOI 4 and 8), posterior auricular aspects of the ilium (VOI 7), and the inferior body (VOI 18–20). The thickest trabeculae are located at the caudal auricular volume (VOI 12 and 13), trabecular chiasma (VOI 14 and 15), and greater sciatic notch (VOI 17).

Trabecular separation (Tb.S)

Trabecular separation within the neonatal ilium can be defined by three different groupings (Figs 5 and 7C). Volumes of interest contributing to a single group display no statistical difference between values (Table 2C). Values are lowest in the superior perimeter (VOI 1, 2 and 6), posterior auricular (VOI 3), superior and central body (VOI 5 and 10), anterior perimeter (VOI 11 and 16), and the acetabular component of the ilium (VOI 21–23). Increased values of trabecular separation are observed in the cranial limb of the auricular surface and surrounding volumes (VOI 4, 7 and 8), central body (VOI 9), and in the inferior body (VOI 18–20). The final and largest value of average trabecular separation is observed to be located in the

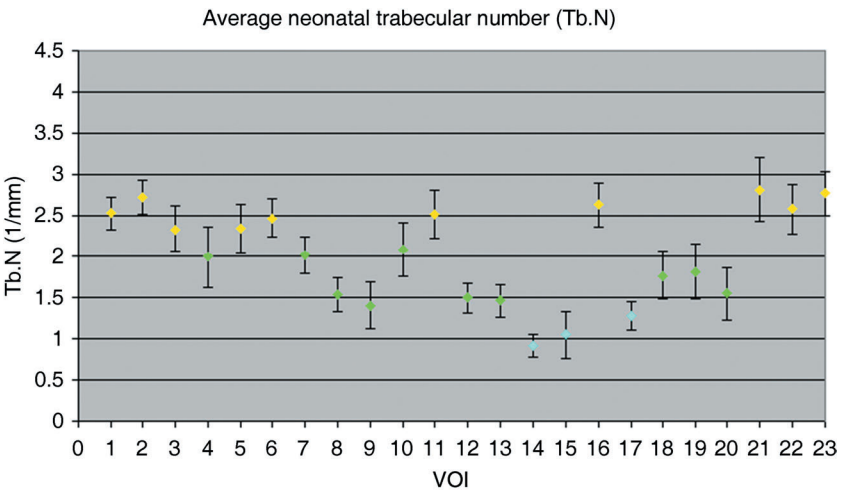

Fig. 6 Graphic representation of mean (± SD) trabecular number at each volume of interest.

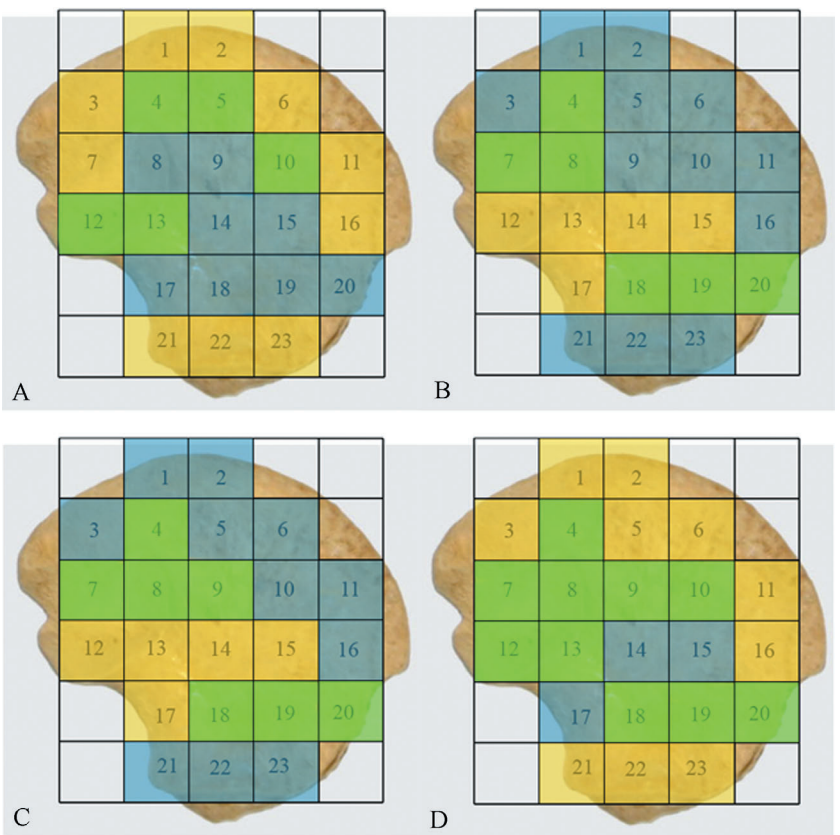

Fig. 7 Coloured map representing regional groupings with statistically similar trabecular characteristics taken from Table 2A–D. (A) High (yellow), medium (green), low (blue) bone volume fraction (BV/TV). (B) High (yellow), medium (green), low (blue) trabecular thickness (Tb.Th). (C) High (yellow), medium (green), low (blue) trabecular separation (Tb.Sp). (D) High (yellow), medium (green), low (blue) trabecular number (Tb.N).

caudal limb of the auricular surface (VOI 12 and 13), the trabecular chiasma region (VOI 14 and 15), and the sciatic notch region (VOI 17).

Trabecular number (Tb.N)

Trabecular number within the neonatal ilium can be defined by three different groupings (Figs 6 and 7D). Volumes of interest contributing to a single group display no statistical difference between values, with one minor exception (Table 2D). The highest trabecular number is observed in the superior perimeter (VOI 1, 2 and 6), posterior auricular (VOI 3), superior body (VOI 5), anterior perimeter regions (VOI 11 and 16), and in the acetabular component of the ilium (VOI 21–23). Reduced trabecular number is observed in regions corresponding to the superior body volume (VOI 4), posterior auricular (VOI 7), cranial and caudal auricular volumes (VOI 8, 12 and 13), the central

body (VOI 9 and 10) and inferior body regions (VOI 18–20). The final and lowest value of average trabecular number is observed in the trabecular chiasma (VOI 14 and 15), and greater sciatic notch region (VOI 17).

Discussion

The skeleton continuously undergoes remodelling throughout life (Hadjidakis & Androulakis, 2006) from early embryonic modelling to the constantly changing architecture of the adult skeleton. However, the rate of bone remodelling during the neonatal period and during the first 2 years of life is much higher than is exhibited in the adult, with neonatal remodelling estimated at 50% *per annum* compared to 5% *per annum* in the adult (Walker, 1991). With emphasis on this and with the knowledge that bone is highly responsive to stress in that it is laid down and remodelled at sites of increased mechanical force or microdamage (Evans, 1957; Turner, 1998; Raisz, 1999; Huiskes et al. 2000), it has been proposed that trabecular characteristics in the ilium may be explained predominantly in terms of direct stance-related bipedal weight transfer and associated ground reaction forces. However, it has become apparent that there is a significant degree of organization of trabecular morphology in the neonatal ilium prior to any possible direct locomotive forces. Trabecular characteristics are aligned in radiating trajectories that essentially mirror those observed in the adult. Therefore, this characteristically mature patterning must be explained by other factors. Discussion of regional trabecular characteristics will be made and paralleled with the radiographic observations of Cunningham & Black (2009).

Ossification of the ilium is first observed between the end of the second and beginning of the third intra-uterine month (Bardeen, 1905; Adair, 1918; Noback, 1944; Gardner & Grey, 1950; Noback & Robertson, 1951; O'Rahilly & Gardner, 1975), within the perichondrium, superior to the future greater sciatic notch (Laurenson, 1964). Initial appositional ossification in the ilium proceeds to spread in a cranial direction on both the gluteal and pelvic surfaces of the iliac blades, without invading the underlying cartilage (Delaere et al. 1992). Subsequently, endochondral ossification, which forms the future trabecular bone within the ilium, commences when pores develop in the ossified external shell, allowing invading osteoblasts and vascular elements to enter the internal disintegrating cartilage matrix, attracted by resultant angiogenic factors (Alini et al. 1996). The recognized point of primary ossification, and the concomitant location of nutrient invasion, observed anterior-superior to the greater sciatic notch (Laurenson, 1964), at a landmark termed the trabecular chiasma, can be demonstrated radiographically by increased bone density. This region displays greater density than surrounding regions due to its advanced ossification resulting in an increased mineral component characterized by increased radiopacity. The resultant progression of endochondral ossification from this centre can then be observed to radiate superiorly into the iliac blade and inferiorly into the acetabular component, illustrated by a distinctive remodelling gradient radiographically (Fig. 8). As such, most recent ossification is located furthest away from the centre of ossification and consequently the most remodelled bone is located furthest away from the growth fronts. Continuous growth of the ilium proceeds by modelling at the growth plates. Therefore, it is necessary, to permit a full explanation of how growth and normal ossification may produce the trabecular characteristics observed in the iliac growth plates, to consider the ilium as a diaphysis with two growing metaphyseal fronts: the iliac crest and the acetabular component.

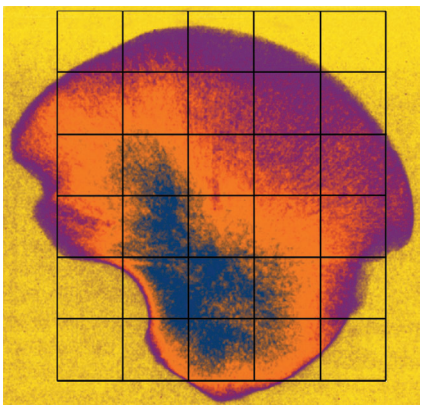

Fig. 8 Gradient enhanced radiograph of neonatal ilium. Radiopacity is illustrated by high values (blue), intermediate values (orange), and low values (magenta). Primary centre of ossification located in blue region with proceeding ossification radiating cranially and caudally represented by colour gradient.

Superior perimeter, anterior perimeter and acetabulum (VOI 1, 2, 6, 11, 16, 21–23)

The trabecular morphology observed in these volumes of interest is characterized by a high bone volume fraction consisting of a high number of thin, tightly packed trabeculae. This structural conformation is considered to be representative of normal early trabecular modelling and related to ossification of the cartilage septae in the hypertrophic zone (Byers et al. 2000). During normal bone proliferation, growth plate cartilage transforms via endochondral ossification into new trabecular bone, where there is a close relationship between the growth plate matrix structure and the newly forming trabecular structure (Rodriguez et al. 1992; Byers et al. 2000). This combined with the fact that the process of endochondral ossification sets the basic trabecular bone scaffold upon which all subsequent modelling and remodelling occurs (Gosman & Ketcham, 2008) allows for an understanding of

growth plate trabecular architecture. In the perimeter growth regions, at the iliac crest and acetabular component, it is suggested that when the primary spongiosa is formed from the calcified cartilage matrix it is laid down in an initial pure form characterized by the structural parameters observed. It is proposed that at the growing fronts, the newly formed trabeculae have had limited exposure to intrinsic forces and therefore limited opportunity to remodel and resorb into a more functionally aligned mature arrangement.

Superior and inferior body (VOI 4, 5, 18–20)

In the superior and inferior body of the ilium, marginal changes in trabecular characteristics from those observed in the perimeter and acetabular regions are apparent. The superior body can be generalized as displaying moderately high trabecular bone volume fraction consisting of a high to medium number of thin, moderately packed trabeculae. Further to this, the inferior body is characterized by a medium to low trabecular bone volume fraction consisting of a low number of moderately spaced thin trabeculae. These alterations from the pattern seen at the growth front most likely represent the effects of remodelling, which can only have occurred in response to *in utero* intrinsic influences as these changes pre-date the more recent pattern seen in the perimeter regions of the neonate. Therefore, the superior and inferior body regions are likely to represent the most recently remodelled regions behind the growth fronts. This remodelling, in regions parallel to the growth fronts, may be in response to a host of influences which may act in unison or in isolation. Direct muscle activity may transmit a force component into the underlying trabeculae, causing a resultant remodelling. Muscular interactions have been shown to have an influence on the trabecular architecture from as early as the fetal period with studies in the fetal ilium suggesting that intrauterine muscular-related biomechanical constraints may have a bearing on certain trabecular characteristics (McColl et al. 2006). Further to this, responses to transferred forces from early reflexive limb movement may account for some aspects of the remodelling observed in the inferior body of the ilium (Cunningham & Black, 2009). Finally, maturation of internal anatomical tissues such as vascular channels and the formation of marrow spaces may have influenced the approximated trabecular characteristics (Crock, 1996). This pattern of graded change in trabecular architecture can be paralleled with the radiographic representation where the superior and inferior body displays a changed morphology concomitant with the proposed local forces. These areas of bone patterning can also be observed radiographically in the adult morphology (Cunningham & Black, 2009); however, the forces determining this morphology have yet to be investigated fully.

Central body (VOI 9 and 10)

The central body of the ilium has a trabecular arrangement characterized by a low bone volume fraction consisting of a medium to low number of thin moderately spaced trabeculae. The central body can be viewed as being the subsequent remodelled front behind the superior body, therefore reinforcing the theory of a remodelling gradient, radiating from the ossification centre, at the trabecular chiasma, towards the periphery. This architectural arrangement may be explained in terms of hypothetical directional force trajectories entering the ilium in a retrograde fashion, from early reflexive limb movement, converging upon the trabecular chiasma and continuing in anterior-superior and postero-superior directions (Cunningham & Black, 2009). In taking this course, these hypothesized forces essentially bypass the central body of the ilium, resulting in a low bone volume fraction combined with weak trabecular characteristics. This can be paralleled with an area of structural redundancy highlighted in radiographic studies (Fig. 8). This area of structural redundancy is also visible in the adult and represents an area of the iliac blade where the gluteal and pelvic shells of compact bone may fuse without any intervening cancellous bone (Cunningham & Black, 2009).

Trabecular chiasma (VOI 13–15)

The trabecular chiasma represents volumes of significantly altered trabecular morphology (Fig. 9). These volumes are characterized by low trabecular bone volume fraction consisting of a very low number of thickened, well-spaced trabeculae. Theoretically, the trabecular chiasma is the most mature region of trabecular bone in terms of proceeding

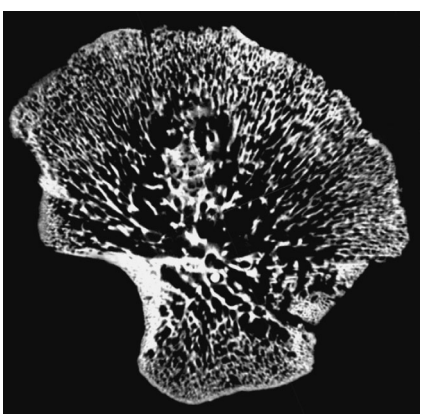

Fig. 9 2D μCT sagittal slice through neonatal ilium illustrating trabecular characteristics across the trabecular volume in one plane. Trabecular characteristics at the centre of ossification, the trabecular chiasma region, reflect the site of nutrient invasion and subsequent radiation of vascular branches into the iliac blade and acetabular component.

ossification in relation to the original location of the primary centre of ossification (Laurenson, 1964; Scheuer & Black, 2000), and the location for highest concentration of vascular channels (Crock, 1996). Therefore, this trabecular arrangement can most likely be attributed to an increase in the functional interactions acting at this region during the fetal and neonatal period from both anatomical (Brandi & Collin-Osdoby, 2006; Eriksen et al. 2007) and biomechanical sources (Walker, 1991, Thelen et al. 2002; Pitsillides, 2006; Nowlan et al. 2007), as well as reflecting the most mature location for remodelling. Although a low value of trabecular bone volume is observed which may initially be considered a feature of structural weakness, the trabecular indices which contribute to this BV/TV are characteristic of increased strength. This architecturally strong conformation can be paralleled with the dense trabecular chiasma observed by plane plate radiography and has previously been attributed to the retrograde forces transferred into the ilium from early reflexive limb movement during the fetal and neonatal periods (Cunningham & Black, 2009). The low bone volume fraction in this region, combined with the dense radiographic representation reported previously, suggests that the cortical shell may make a significant contribution to the structural integrity of the trabecular chiasma as a region of increased neonatal force transmittance. This theory is reinforced by the understanding that the ilium is a 'sandwich structure' consisting of low density trabecular bone covered by layers of thin cortical bone forming a strong, low-weight structure that is well suited to accommodate high loads (Dalstra & Huiskes, 1995). This region of strengthened trabecular characteristics and overall increased bone density representation can be paralleled with the adult representation (Macchiarelli et al. 1999; Rook et al. 1999).

Auricular surface (VOI 8 and 12)

The cranial (VOI 8) and caudal (VOI 12) auricular regions differ in their trabecular characteristics. Volumes of interest relevant to the cranial auricular surface present with a trabecular morphology characterized by a medium to low trabecular bone volume fraction consisting of a relatively low number of thin, moderately spaced trabeculae. This is a similar morphology to the adjacent central body. The trabecular morphology in the caudal auricular surface presents as a medium to high trabecular bone volume fraction consisting of a low number of thickened, well-spaced trabeculae. This is a similar morphology to the adjacent posterior region of the trabecular chiasma. In all trabecular parameters except Tb.N there appears to be a difference in trabecular morphology between these volumes; however, none of these differences reaches a statistically significant level. Therefore, although the cranial morphology is more similar to the appearance of the central body and the caudal limb to the chiasma trabecular morphology, they are essentially consistent within the morphology of their adjacent regions. As such, there is no evidence to suggest selective remodelling in the internal architecture related to this joint. The overall architectural arrangement observed in these volumes may be attributed to functional influences on the joint during the neonatal period. Immediate focus in this case is directed towards the ligamentous associations which will already be well developed, having been recognizable surrounding the articular surfaces from 20 intrauterine weeks (Salsabili & Hogg, 1991). It is proposed that stresses and strains induced by the strong ligamentous interactions which encapsulate the joint (Bowen & Cassidy, 1981; Vleeming et al. 1990) may cause a gradual remodelling process within the underlying trabecular bone, causing the changes in the auricular and surrounding volumes of interest.

Greater sciatic notch (VOI 17)

Trabecular morphology in the greater sciatic notch volume of interest is characterized by a medium to low trabecular bone volume fraction consisting of a very low number of thickened, well-spaced trabeculae. Again consideration is given to immediate soft tissue structures and in particular to the large and closely approximated sciatic nerve. It is possible that neurogenic influences from this nerve may alter the morphology of the underlying trabeculae. Indeed, proximity of nervous tissue has been considered to be responsible for thickening of the cortical shell as a protective mechanism to the sciatic nerve and thought has also been given to the potential for neurogenesis being an initiator of endochondral ossification in the ilium (Laurenson, 1964; Scheuer & Black, 2000). If neurogenic influences can induce profound changes in bone it may be possible that the significantly altered trabecular characteristics within the sciatic notch volume, consisting of low trabecular bone volume fraction combined with a very low number of thickened, well-spaced trabeculae, may in part be attributable to this. Recent studies have also highlighted that the metabolic control of bone is influenced heavily by the nervous system (Jones et al. 2004). When paralleling the structural quantification in the sciatic notch region to the radiographic representation, further inferences can be made regarding the structural composition of this region and the potential contribution to this strength from the sciatic nerve. This region was represented as an area of increased structural density radiographically, which parallels the trabecular phenotype of increased thickening of structurally significant trabeculae in order to confer strength and protection (Figs 8 and 9). This region is also reputedly an area of particular strength in the adult due to the passage of the sacro-ischial trabecular bundle (Aiello & Dean, 1990, Scheuer & Black, 2000). Further investigation in relation to

cortical thickness is required to consider the inter-relationship with internal architecture.

Although it is likely that normal growth combined with local anatomical and biomechanical influences have a predominant and marked influence on trabecular characteristics, consideration must also be given to the potential genetic influences which act upon the trabecular architecture and the skeleton as a whole. It is feasible that a predetermined genetic template of trabecular structure may be evident and thus a precocious development of progressive organized trabecular architecture may ensue. This genetic template may then be acted upon and altered by various mechanical, anatomical, angiogenic and neurogenic factors to shape the trabecular architecture into an optimal conformation for a particular temporal developmental window. Thus a potential genetic component of early trabecular architectural organization may act as a preparatory mechanism, in unison with proposed extra-genetic influences, enabling the structural composition of the ilium to accommodate a life-time of functionally inherent ontogenetic stresses and strains.

Conclusion

This study revealed that a recognizable and regional organization of internal cancellous architecture is established at a very early maturational stage in the human ilium. Remarkably, the observed morphology can be paralleled with the generalized patterning observed in the adult, which is more usually and specifically attributed to locomotive influences. As such, the early presence of this mature trabecular morphology suggests that previous attribution of iliac trabecular patterning to locomotor weight transfer may be too simplistic. Therefore, other factors including progressive remodelling in response to normal growth and ossification, inherent anatomical interactions and early reflex limb movement must be considered. It is therefore suggested that the neonatal trabecular pattern may yet yield an insight into the developmental origins of future load-bearing structures. Further to this, it must also be postulated that the observed patterning may be indicative of a predetermined template upon which early non-weight bearing and later, stance-related, locomotive influences may be superimposed and perhaps reinforced at a later age. This study contributes to a greater understanding of early developmental trabecular organization in the ilium and has core implications for understanding the origins of trabecular characteristics attributed to load-bearing structures in the adult by providing a foundation for subsequent ontogenetic development.

Acknowledgements

Thanks are given to Dr Michael Fagan and colleagues from the University of Hull for providing micro-computed tomography equipment which was essential to the completion of this study. Grant support from the Biotechnology and Biological Sciences Research Council (BBSRC) is gratefully acknowledged.

References

Adair FL (1918) The ossification centres of the fetal pelvis. *Am J Obst Dis Women Chil* **78**, 175–199.

Aiello L, Dean C (1990) *An Introduction to Human Evolutionary Anatomy*. London: Academic Press.

Alini M, Marriott A, Chen T, Abe S, Poole R (1996) A novel angiogenic molecule produced at the time of chondrocyte hypertrophy during endochondral bone formation. *Dev Biol* **176**, 124–132.

Bardeen CR (1905) Studies of the development of the human skeleton. *Am J Anat* **4**, 265–302.

Bevill G, Eswaran SK, Gupta A, Papadopoulos P, Keaveny TM (2006) Influence of bone volume fraction and architecture on computed large-deformation failure mechanisms in human trabecular bone. *Bone* **39**, 1218–1225.

Biewener AA, Fazzalari NL, Konieczynski DD, Baudinette RV (1996) Adaptive changes in trabecular architecture in relation to functional strain patterns and disuse. *Bone* **19**, 1–8.

Bowen V, Cassidy JD (1981) Macroscopic and microscopic anatomy of the sacroiliac joint from embryonic life until the eighth decade. *Spine* **6**, 620–628.

Boyd SK, Davison P, Muller R, Gasser JA (2006) Monitoring individual morphological changes over time in ovariectomized rats by *in vivo* micro-computed tomography. *Bone* **39**, 854–862.

Brandi ML, Collin-Osdoby P (2006) Vascular biology and the skeleton. *J Bone Min Res* **21**, 183–192.

Byers S, Moore AJ, Byard RW, Fazzalari NL (2000) Quantitative histomorphometric analysis of the human growth plate from birth to adolescence. *Bone* **27**, 495–501.

Carter DR, Hayes WC (1977) The compressive behaviour of bone as a two phase porous structure. *Am J Bone Joint Surg* **59**, 954–962.

Chappard D, Legrand E, Pascaretti C, Baslé MF, Audran M (1999) Comparison of eight histomorphometric methods for measuring trabecular bone architecture by image analysis on histological sections. *Microsc Res Tech* **45**, 303–312.

Ciarelli MJ, Goldstein SA, Kuhn JL, Cody DD, Brown MB (1991) Evaluation of orthogonal mechanical properties and density of human trabecular bone from the major metaphyseal regions with materials testing and computed tomography. *J Orthopaed Res* **9**, 674–682.

Compston J (2006) Bone quality: What is it and how is it measured? *Arq Bras Endocrinol Metabol* **50**, 579–585.

Cooper DML, Turinsky AL, Sensen CW, Hallgrimsson B (2003) Quantitative 3D analysis of the canal network in cortical bone by micro-computed tomography. *Anat Rec B New Anat* **274**(B), 169–179.

Crock HV (1996) *An Atlas of Vascular Anatomy of the Skeleton & Spinal Cord*. London: Martin Dunitz.

Cunningham CA, Black SM (2009) Development of the fetal ilium – challenging concepts of bipedality. *J Anat* **214**, 91–99.

Dalle Carbonare L, Valenti MT, Bertoldo F, et al. (2005) Bone microarchitecture evaluated by histomorphometry. *Micron* **36**, 609–616.

Dalstra M, Huiskes R (1995) Load transfer across the pelvic bone. *J Biomech* **28**, 715–724.

Dalstra M, Huiskes R, Odgaard A, Van Erning L (1993) Mechanical

and textural properties of pelvic trabecular bone. *J Biomech* **26**, 523–535.

Delaere O, Kok V, Nyssen-Behets C, Dhem A (1992) Ossification of the human fetal ilium. *Acta Anat* **143**, 330–334.

Ding M, Odgaard A, Hvid I (1999) Accuracy of cancellous bone volume fraction measured by micro-CT scanning. *J Biomech* **32**, 323–326.

Ding M, Day JS, Burr D, et al. (2003) Canine cancellous bone microarchitecture after one year of high dose bisphosphonates. *Calcified Tissue Int* **72**, 737–744.

Eriksen EF, Eghbali-Fatourechi GZ, Khosla S (2007) Remodeling and vascular spaces in bone. *J Bone Min Res* **22**, 1–6.

Evans FG (1957) *Stress and Strain in Bones.* Springfield, IL: Charles C Thomas.

Evans FG (1973) *Mechanical Properties of Bone*. Springfield, IL: Charles C Thomas.

Fajardo RJ, Muller R (2001) Three-dimensional analysis of non-human primate trabecular architecture using micro-computed tomography. *Am J Phys Anthropol* **115**, 327–336.

Fajardo RJ, Ryan TM, Kappelman J (2002) Assessing the accuracy of high-resolution X-ray computed tomography of primate trabecular bone by comparisons with histological sections. *Am J Phys Anthropol* **118**, 1–10.

Fazekas IGy, Kosa F (1978) *Forensic Fetal Osteology.* Budapest: Akademiai Kiado.

Frost HM (1990) Skeletal structural adaptations to mechanical usage (SATMU): redefining Wolff's law: The bone modelling problem. *Anat Rec* **226**, 403–413.

Gardner E, Grey DJ (1950) Prenatal development of the human hip joint. *Am J Anat* **87**, 163–211.

Genant HK, Gordon C, Jiang Y, et al. (2000) Advanced imaging of macrostructure and microstructure of bone. *Hormone Res* **54**, 24–30.

Gibson LJ (1985) The mechanical behaviour of cancellous bone. *J Biomech* **18**, 317–328.

Glorieux FH, Travers R, Taylor A, et al. (2000) Normative data for iliac bone histomorphometry in growing children. *Bone* **26**, 103–109.

Goldstein SA (1987) The mechanical properties of trabecular bone: dependence on anatomic location and function. *J Biomech* **20**, 1055–1061.

Gosman JH, Ketcham RA (2008) Patterns in ontogeny of human trabecular bone from SunWatch Village in the prehistoric Ohio Valley: general features of microarchitectural change. *Am J Phys Anthropol* **138**, 318–322.

Hadjidakis DJ, Androulakis II (2006) Bone remodeling. *Ann NY Acad Sci* **1092**, 385–396.

Hildebrand T, Ruegsegger P (1997) A new method for the model independent assessment of thickness in three dimensional images. *J Microsc* **185**, 67–75.

Hildebrand T, Laib A, Muller R, Dequeker J, Ruegsegger P (1999) Direct three-dimensional morphometric analysis of human cancellous bone: Microstructural data from spine, femur, iliac crest, and calcaneus. *J Bone Min Res* **14**, 1167–1174.

Huiskes R, Ruimerman R, van Lenthe G, Janssen JD (2000) Effects of mechanical forces on maintenance and adaptation of form in trabecular bone. *Nature* **405**, 704–706.

Jee WS (2005) The past, present, and future of bone morphometry: its contribution to an improved understanding of bone biology. *J Bone Min Metabol* **23**(S), 1–10.

Jones KB, Mollano AV, Morcuende JA, Cooper RR, Saltzman CL (2004) Bone and brain: A review of neural, hormonal, and musculoskeletal connections. *Iowa Orthop J* **24**, 123–132.

Jones JR, Poologasundarampillai G, Atwood RC, Bernard D, Lee PD (2007) Non-destructive quantitative 3D analysis for the optimization of tissue scaffolds. *Biomaterials* **28**:1404–1413.

Keaveny TM, Morgan EF, Niebur GL, Yeh OC (2001) Biomechanics of trabecular bone. *Ann Rev Biomed Eng* **3**, 307–333.

Kim DG, Christopherson GT, Dong XN, Fyhrie DP, Yeni YN (2004) The effect of microcomputed tomography scanning and reconstruction voxel size on the accuracy of stereological measurements in human cancellous bone. *Bone* **35**, 1375–1382.

Laib A, Kumer JL, Majumdar S, Lane NE (2001) The temporal changes of trabecular architecture in ovariectomized rats assessed by microCT. *Osteop Int* **12**, 936–941.

Lanyon LE (1974) Experimental support for the trajectorial theory of bone structure. *J Bone Joint Surg* **56B**, 160–166.

Laurenson RD (1964) The primary ossification of the human ilium. *Anat Rec* **148**, 209–217.

Liu XS, Sajda P, Saha PK, Wehrli FW, Guo XE (2006) Quantification of the roles of trabecular architecture and trabecular type in determining the elastic modulus of human trabecular bone. *J Bone Min Res* **21**, 1608–1617.

Macchiarelli R, Bondioli L, Galichon V, Tobias PV (1999) Hip bone trabecular architecture shows uniquely distinctive locomotor behaviour in South African australopithecines. *J Hum Evol* **36**, 211–232.

Macho GA, Abel RL, Schutkowski H (2005) Age changes in bone microstructure: do they occur uniformly? *Int J Osteoarcheol* **15**:421–430.

Majumdar S, Kothari M, Augat P, et al. (1998) High-resolution magnetic resonance imaging: three-dimensional trabecular bone architecture and biomechanical properties. *Bone* **22**, 445–454.

Majumder S, Roychowdhury A, Pal S (2004) Variations of stress in pelvic bone during normal walking, considering all active muscles. *Trends Biomater Artif Organs* **17**, 48–53.

Martinon-Torres M (2003) Quantifying trabecular orientation in the pelvic cancellous bone of modern Humans, Chimpanzees, and the Kebara 2 Neanderthal. *Am J Hum Biol* **15**, 647–661.

McColl DJ, Abel R, Spears IR, Macho GA (2006) Automated method to measure trabecular thickness from microcomputed tomographic scans and its application. *Anat Rec A Discov Mol Cell Evol Biol* **288A**, 982–988.

Moore RJ, Durbridge TC, Woods AE, Vernon-Roberts B (1989) Variation in histomorphometric estimates across different sites of the iliac crest. *J Clin Pathol* **42**, 814–816.

Mulder L, van Ruijven LJ, Koolstra JH, van Eijden TMGJ (2007) Biomechanical consequences of developmental changes in trabecular architecture and mineralization of the pig mandibular condyle. *J Biomech* **40**, 1575–1582.

Müller R (2005) Long-term prediction of three-dimensional bone architecture in simulations of pre-, peri- and post-menopausal microstructural bone remodelling. *Osteoporosis Int* **16**, S25–S35.

Müller R, Van Lenthe GH (2006) Trabecular bone failure at the microstructural level. *Cur Osteoporosis Rep* **4**, 80–86.

Müller R, Van Campenhout H, Van Damme B, et al. (1998) Morphometric analysis of human bone biopsies: a quantitative structural comparison of histological sections and micro-computed tomography. *Bone* **23**, 59–66.

Nagaraja S, Lin ASP, Guldberg RE (2007) Age-related changes in trabecular bone microdamage initiation. *Bone* **40**, 973–980.

Nakano H, Watahiki J, Kubota M, et al. (2003) Micro X-ray computed tomography analysis for the evaluation of asymmetrical condylar growth in the rat. *Orthod Craniofac Res* **6**(Suppl. 1), 168–172.

Noback CR (1944) The developmental anatomy of the human osseous skeleton during ht eembryonic, fetal and circumnatal periods. *Anat Rec* **88**: 91–125.

Noback CR, Robertson GG (1951) Sequences of appearance of ossification centres in the human skeleton during the first five prenatal months. *Am J Anat* **89**, 1–28.

Nowlan NC, Murphy P, Prendergast PJ (2007) Mechanobiology of embryonic limb development. *Ann NY Acad Sci* **1101**, 389–411.

Nuzzo S, Meneghini C, Braillon P, Bouvier R, Mobilio S, Peyrin F (2003) Microarchitectural and physical changes during fetal growth in human vertebral bone. *J Bone Min Res* **18**(4), 760–768.

O'Rahilly R, Gardner E (1975) The timing and sequence of events in the development of the limbs in the human embryo. *Anat Embryol* **148**, 1–23.

Parfitt AM, Drezner MK, Glorieux FH, Kanis JA, Malluche H, Meunier PJ (1987) Bone histomorphometery: standardization of nomenclature, symbols, and units. *J Bone Min Res* **2**, 595–610.

Patel PV, Prevrhal S, Bauer JS, et al. (2005) Trabecular bone structure obtained from multislice spiral computed tomography of the calcaneus predicts osteoporotic vertebral deformities. *J Comp Assisted Tomogr* **29**, 246–253.

Petersson J, Brismar T, Smedby O (2006) Analysis of skeletal microstructure with clinical multislice CT. *Med Image Comp Comp Assisted Interv: MICCAI* **9**, 880–887.

Pierroz DD, Bouxsein ML, Rizzoli R, Ferrari SL (2006) Combined treatment with a beta-blocker and intermittent PTH improves bone mass and microarchitecture in ovariectomized mice. *Bone* **39**, 260–267.

Pitsillides AA (2006) Early effects of embryonic movement: 'a shot out of the dark'. *J Anat* **208**, 417–431.

Qin L, Genant HK, Griffith J, Leung KS (2007) *Advanced Bioimaging Techniques in Assessment of the Quality of Bone and Scaffold Materials, Techniques and Application*, pp. 79–84. Berlin: Springer.

Raisz LG (1999) Physiology and pathophysiology of bone remodeling. *Clinl Chem* **45**(8B), 1353–1358.

Ripamonti U (2006) Soluble osteogenic molecular signals and the induction of bone formation. *Biomaterials* **27**, 807–822.

Ritman EL (2004) Micro-computed tomography-current status and developments. *Ann Rev Biomed Eng* **6**, 185–208.

Rodriguez JI, Razquin S, Palacios J, Rubio V (1992) Human growth plate development in the fetal and neonatal period. *J Orthop Res* **10**, 62–71.

Rook L, Bondioli L, Kohler M, Moya-Sola S, Macchiarelli R (1999) *Oreopithecus* was a bipedal ape after all: evidence from the iliac cancellous architecture. *Proc Natl Acad Sci U S A* **96**, 8795–8799.

Ryan TM, Ketcham RA (2002) Femoral head trabecular bone structure in two omomyid primates. *J Hum Evol* **43**, 241–263.

Ryan TM, Krovitz GE (2006) Trabecular bone ontogeny in the human proximal femur. *J Hum Evol* **51**, 591–602.

Ryan TM, van Rietbergen B (2005) Mechanical significance of femoral head trabecular bone structure in Loris and Galagos evaluated using micromechanical finite element analysis. *Am J Hum Evol* **126**, 82–96.

Salsabili N, Hogg DA (1991) Development of the human sacroiliac joint. *Clin Anat* **4**, 99–108.

Saparin P, Thomsen JS, Kurths J, Beller G, Gowin W (2006) Segmentation of bone CT images and assessment of bone structure using measures of complexity. *Med Phys* **33**, 3857–3873.

Scheuer L, Black S (2000) *Developmental Juvenile Osteology*. London: Academic Press.

Stauber M, Müller R (2006) Age-related changes in trabecular bone microstructures: global and local morphometry. *Osteoporosis Int* **17**, 616–626.

Stauber M, Müller R (2008) Microcomputed tomography: a method for the non-destructive evaluation of the three dimensional structure of biological specimens. *Methods Mol Biol* **455**, 273–292.

Thelen E, Fisher DM, Ridley-Johnson R (2002) The relationship between physical growth and newborn reflex. *Inf Behav Devel* **25**, 72–85.

Thomsen JS, Ebbesen EN, Mosekilde LI (2002) Static histomorphometry of human iliac crest and vertebral trabecular bone: a comparative study. *Bone* **30**, 267–274.

Turner CH (1998) Three rules for bone adaptation to mechanical stimuli. *Bone* **23**, 339–409.

Ulrich D, van Rietbergen B, Laib A, Ruegsegger P (1999) The ability of three-dimensional structural indices to reflect mechanical aspects of trabecular bone. *Bone* **25**, 55–60.

Vleeming A, Stoeckart R, Volkers ACW (1990) Relation between form and function in the sacroiliac joint (I): the clinical anatomical aspects. (II): the biomechanical aspects. *Spine* **15**, 130–132.

Von Mayer HV (1867) Die Architectur der Spongiosa. *Reickert und du Bois-Reymond's Arch* 627.

Walker JM (1991) Musculoskeletal development: a review. *Physl Ther* **71**, 878–889.

Ward FO (1838) *Outlook of Human Osteology*. London: Renshaw.

Whitehouse WJ (1974) The quantitative morphology of anisotropic trabecular bone. *J Microsc* **101**, 153–168.

Wolff J (1892) *Das Gesetz der Transformation der Knochen*. Berlin: Verlag von August Hirschwald.

Wolff J (1986) *The Law of Bone Remodelling*. Berlin: Springer-Verlag. [Translated by P. Maquet and R. Furlong from the original (1892)].